Preparation and Characterization of Polymer−Inorganic Nanocomposites by In Situ Melt Polycondensation of L-Lactic Acid and Surface-Hydroxylated MgO

Yonghui Li and Xiuzhi Susan Sun*

Bio-Materials and Technology Lab, Department of Grain Science and Industry, Kansas State University, Manhattan, Kansas 66506

Received March 22, 2010; Revised Manuscript Received May 18, 2010

Compared with pristine polymers, bionanocomposites derived from biopolymers and inorganic nanoparticles have significantly improved electrical/magnetic properties, mechanical properties, thermal stability, gas barrier properties, and fire retardance. In this study, poly(lactic acid) (PLA) nanocomposites were prepared by in situ melt polycondensation of L-lactic acid with different loading ratios of surface-hydroxylated magnesium oxide (MgO) nanocrystals. Molecular weight, structure, morphology, and thermal properties of the nanocomposites were characterized. PLA-grafted MgO (PLA-*g*-MgO) was isolated from free PLA for the nanocomposite with 3% MgO via repeated dispersion/centrifugation processes and characterized. The weight-average molecular weight of the PLA-0.01%MgO nanocomposite was 55500, which was 30% higher than that of pure PLA. Discoloration of PLA was obviously depressed in the presence of MgO nanocrystals. Formation of hydrogen bonding between PLA chains and surface −OH groups from MgO was detected by Fourier transform infrared spectroscopy. Morphological images showed uniform dispersion of MgO nanocrystals in the PLA matrix and demonstrated a strong interfacial interaction between the PLA matrix and MgO nanocrystals. PLA-MgO nanocomposites exhibited improved thermal stability compared with pure PLA. Calculations based on thermogravimetric analysis revealed that more than 42.5% PLA was successfully grafted into PLA-*g*-MgO.

Introduction

Poly(L-lactic acid) (PLA), a biodegradable and compostable polymer made from renewable resources such as corn starch, has been extensively studied in recent years as an alternative to petrochemical plastics. It has shown great potential to produce biomedical materials, textiles, films, vehicle interiors, appliance components, service utensils, and packaging materials.[1–4] However, unsatisfactory characteristics of PLA such as modest strength and modulus, brittleness, low modulus at glass transition temperature around 60 °C, poor gas barrier properties, and slow crystallization rate have limited its use. The study of polymer−inorganic nanocomposites is of great interest to both industry and academia because these nanocomposites exhibit significantly improved properties compared with pristine polymers, including electrical/magnetic properties, mechanical properties, thermal stability, gas barrier properties, and fire retardance.[5–12] The development of a nanoscale dispersion of inorganic nanoparticles in the polymer matrix and specific interactions between them are two keys to achieving the best combination of nanocomposite properties.[11,13,14]

Currently, most PLA nanocomposites are prepared by melt blending[15–17] or in situ ring-opening polymerization of lactide.[18–20] However, effective dispersion of nanoparticles in the polymer matrix has been a challenge because nanoparticles agglomerate. The nanoparticle surface is often modified to promote dispersion,[11,21] which frequently results in extra cost and use of toxic organic solvents. In situ ring-opening polymerization of lactide involves the formation and purification of lactide from the oligocondensation of lactic acid, which also increases the cost of PLA production[22,23] and prevents its application in various commodities. A breakthrough technology has recently been reported to produce PLA with moderate molecular weight; this technology is based on the direct melt polycondensation of lactic acid and uses a tin (Sn(II)) catalyst system activated by proton acids.[24,25] It has also been reported that the molecular weight of PLA can further increase to several hundred thousand when the melt polycondensation is subjected to another solid-state postpolycondensation process.[26] Therefore, in this study, we proposed an in situ melt polycondensation strategy to prepare PLA nanocomposites using L-lactic acid (LA) and inorganic nanocrystals (surface-hydroxylated magnesium oxide, MgO) as starting materials.

Of all inorganic nanoparticles, metal oxides (magnesium, aluminum, iron, titanium, silicon, etc.) have attracted much attention because a layer of hydroxyl (−OH) groups that results from water dissociation covers the outmost surface of oxide nanocrystals.[27–29] Silicon dioxide (SiO_2)[30–32] and titanium dioxide (TiO_2)[33] have been studied recently. However, MgO has a much smaller crystal size (≤4 nm) than SiO_2 (∼12 nm) and TiO_2 (∼20 nm) and, thus, should have more surface defects and higher reactivity that should result in higher efficiency of water dissociation, which usually occurs only at defects on oxide surfaces such as corners, edges, steps, kinks, and vacancies.[34,35] In regard to MgO, for each type of defect, two main categories of −OH groups are generally expected from heterolytic dissociation of water:[36–38] (1) −OH groups produced by hydroxylation of surface Mg^{2+} cations (called monocoordinated hydroxyls because they are bonded to only one Mg^{2+} cation) and (2) −OH groups generated by protonation of surface oxide ions (referred to as multicoordinated hydroxyls because they are bonded to several Mg^{2+} cations). Generally, only the low-coordinated (mono- and di-) −OH groups on the edge and corner

* To whom correspondence should be addressed. Tel.: 785-532-4077. Fax: 785-532-7193. E-mail: xss@ksu.edu.

10.1021/bm100320q
Published on Web 06/11/2010

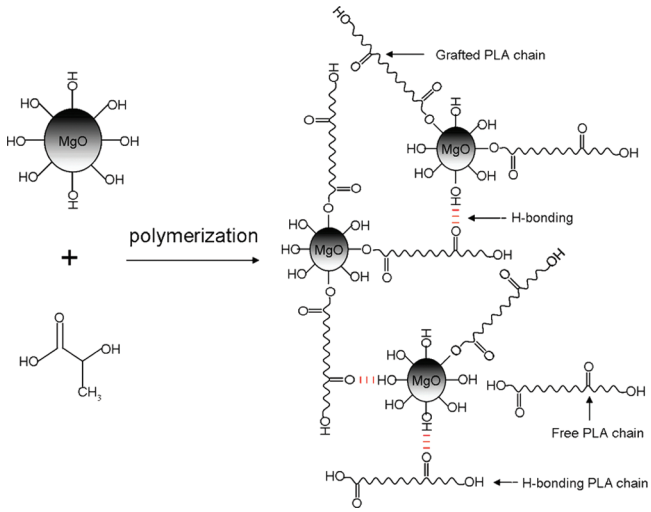

Figure 1. Scheme of the synthesis of PLA/MgO nanocomposites and formation of hydrogen bonding.

sites can be more reactive and are responsible for the reactivity of hydroxylated MgO.[29,36]

The MgO used in this study was provided by NanoScale Co. (NanoActive Magnesium Oxide Plus) following the aerogel method developed by Klabunde and his co-workers.[39,40] The MgO exhibited a polyhedral shape with a much larger surface area (≥600 m^2/g) and percentage of corner and edge ions (21%) than commercial cubic-shaped MgO (surface area: 30 m^2/g, corner and edge ions: 0.4%).[41] The MgO contains about nine −OH groups/nm^2 at 100 °C; the surface −OH group concentration decreased progressively with heat treatment temperature but still possessed an average of 3.6 surface −OH groups/nm^2 after heat treatment at 500 °C under vacuum.[40] Some attention has been paid to the reactivity of this highly hydroxylated MgO in the area of catalysts and adsorbents studies;[41,42] however, limited studies have been conducted for polymer nanocomposites.[17,43] In our previous study, surface-hydroxylated MgO (NanoActive Magnesium Oxide) was used as filler to prepare PLA nanocomposites by melt blending.[17] At an MgO loading ratio of 0.4 wt % or less, mechanical properties were significantly improved, which was mainly attributed to the nanoreiforcement of a large amount of surface −OH groups of MgO. However, satisfying dispersion of MgO in the melt PLA matrix was still not achieved.

In this study, we hypothesized that carbonyl groups from LA could polymerize with hydroxyl groups from surface-hydroxylated MgO crystals to form PLA-MgO nanocomposites (as illustrated in Figure 1) to create better interfacial interaction and dispersion of MgO crystals in the PLA matrix and that interfacial interaction between the PLA matrix and MgO could further be improved through formation of hydrogen bonding (H-bonding) between remaining surface −OH groups of MgO and ester groups in the PLA chains (Figure 1). This study had three specific objectives: (1) synthesize PLA/MgO nanocomposites via in situ melt polycondensation from LA with different MgO loading ratios; (2) characterize the molecular weight, structure, morphology, and thermal properties of bulk nanocomposites; and (3) characterize the properties of PLA-grafted MgO (PLA-*g*-MgO) isolated from free PLA from the PLA-3%MgO nanocomposite to confirm the surface polymerization.

Experimental Section

Materials. L-Lactic acid was supplied as a 90 wt % aqueous solution by Acros Organics. MgO with an extremely high surface area, small crystal size (≤4 nm), and rough surface morphology was obtained from NanoScale Co. (NanoActive Magnesium Oxide Plus, Manhattan, KS). Tin(II) chloride dihydrate ($SnCl_2 \cdot H_2O$; 98%, reagent grade) and *p*-toluenesulfonic acid monohydrate (TSA; 98.5+%, ACS reagent grade) were purchased from Sigma-Aldrich Co. All materials were used as received.

Dehydration/Oligomerization. Our preliminary studies showed that the desirable MgO loading level for bulk nanocomposite preparation was less than 0.2%; this value was used to determine the experimental MgO loading levels (0.005, 0.01, 0.05, and 0.2% based on the weight of pure LA).The MgO was added gradually to 100 g of a 90 wt % aqueous solution of LA and stirred with a magnetic stirrer until it was uniformly dispersed. The mixture was then charged into a 250 mL three-neck flask and dehydrated at 110 °C under atmospheric pressure for 2 h, then at 130 °C under a reduced pressure of 100 Torr for 3 h, and finally at 150 °C under a reduced pressure of 10 Torr for another 4 h. Then a viscous oligomer with MgO was obtained. Oligomer without MgO was also prepared as a control following the same procedures. The degree of polymerization (DP) of the oligomers was determined to be about 6 through ^1H NMR.

Polymerization. A 100 mL three-neck flask was equipped with a mechanical stirrer and a reflux condenser that was connected with a vacuum system through a liquid nitrogen cold trap. A total of 20 g oligomer was charged into the flask and then mixed with $SnCl_2 \cdot H_2O$ (0.4 wt % relative to oligomer) and TSA (an equimolar ratio to $SnCl_2 \cdot H_2O$) as a binary catalyst.[24] The mixture was gradually heated to 180 °C with stirring. The pressure was reduced gradually to 10 Torr in 1.5 h. Then the reaction was continued at 180 °C/10 Torr for 10 h. At the end of the reaction, the flask was cooled, and the product was dissolved in chloroform and subsequently precipitated into methanol. The resulting solid was filtered and dried under vacuum at 80 °C for 24 h. Bulk nanocomposites were labeled according to MgO loading ratio as PLA-0.005%MgO, PLA-0.01%MgO, PLA-0.05%MgO, and PLA-0.2%MgO. Pure PLA without MgO was prepared following the same procedures and used as a control. Because both PLA-*g*-MgO and free PLA in the bulk nanocomposites at 0.2% MgO or lower are dissolved/dispersed completely in chloroform, we prepared a PLA-3%MgO nanocomposite to isolate enough PLA-*g*-MgO for characterization purposes. To prepare the PLA-3%MgO nanocomposite, pure LA oligomer was first prepared following the same dehydration/oligomerization procedures. The 3% MgO was added into 20 g of oligomer and then mixed with the same amount of catalysts and polymerized at the same conditions as other nanocomposites. The 3% MgO was added to the LA oligomer rather than to LA to obtain a higher yield of PLA-*g*-MgO.

Isolation of PLA-*g*-MgO. When the PLA-3%MgO nanocomposite was dispersed into excessive chloroform, free PLA was completely dissolved, and some PLA-*g*-MgO remained. The PLA-*g*-MgO was isolated from free PLA via centrifugation at 8500 rpm for 1 h and washed with excessive chloroform repeatedly five times to completely remove the free PLA. Free PLA from the first centrifugation was precipitated into methanol and collected. A control sample (t-MgO) was also prepared by mixing 1 g MgO with a chloroform solution of PLA for 10 h and then repeating the dispersion/centrifugation cycles. The photographs of PLA-*g*-MgO/free PLA/chloroform and t-MgO/PLA/chloroform suspensions before and after centrifugation are shown in Figure 2. It is clear that t-MgO was precipitated at the bottom of the tube and PLA-*g*-MgO was suspended at the top after centrifugation. This indicates there always will be a certain amount of PLA-*g*-MgO dissolved/dispersed in PLA/chloroform solution and remaining with free PLA after precipitation. Finally, the PLA-*g*-MgO, t-MgO, and free PLA were dried in a vacuum oven at 80 °C for 24 h to remove the residual solvent.

Gel Permeation Chromatography (GPC) Analysis. The weight-(M_w) and number-average molecular (M_n) weight as well as the polydispersity index (PDI, equal to M_w/M_n) were determined through GPC (Waters 2695 separation module). Samples were dissolved in

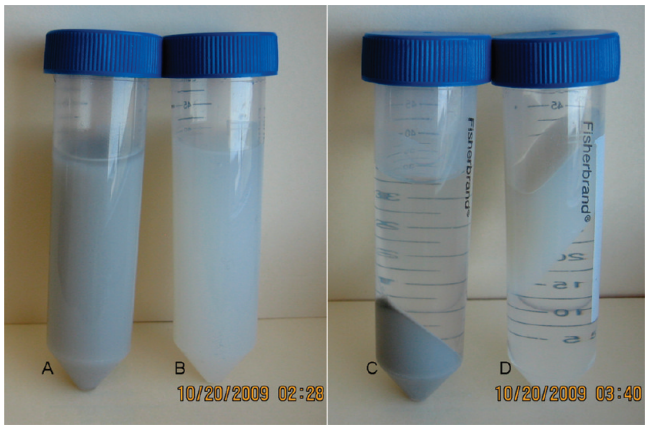

Figure 2. Photograph of t-MgO/PLA/chloroform suspension before (A) and after (C) centrifugation and PLA-*g*-MgO/free PLA/chloroform suspension before (B) and after centrifugation (D).

tetrahydrofuran at a concentration of 5 mg/mL. The measurement was performed at room temperature and a flow rate of 1 mL/min. The molecular weight was calibrated according to a polystyrene standard.

Nuclear Magnetic Resonance (NMR) Spectroscopy. ^{1}H and ^{13}C NMR spectra were acquired at room temperature for PLA and bulk nanocomposites on a Varian Inova 400 MHz spectrometer in $CDCl_3$ containing tetramethylsilane as the internal reference. All spectra were recorded using a spinning rate of 20 kHz with a relaxation delay of 1 s for ^{1}H NMR and 3 s for ^{13}C NMR. Solid-state ^{1}H and ^{13}C NMR spectra were obtained for PLA-*g*-MgO and free PLA isolated from the PLA-3%MgO nanocomposite on a Bruker IPSO 500 MHz WB NMR spectrometer. The ^{1}H NMR was carried out with a single 90° pulse of 1.3 μs under ultrahigh magic-angle spinning (MAS) at 60 kHz. The ^{13}C NMR was performed with cross-polarization MAS under the following conditions: sample spinning rate 10 kHz, contact time 2 ms, relaxation delay 3 s, and two-pulse phase modulation proton decoupling during acquisition.

Fourier-Transform Infrared (FTIR) Spectroscopy. FTIR spectra were acquired with a Perkin-Elmer Spotlight 300 spectrometer. Spectra were collected in the region of 4000−800 cm^{-1} with a spectral resolution of 8 cm^{-1} and 64 scans coadded.

Scanning Electron Microscopy (SEM) and Transmission Electron Microscopy (TEM) Analysis. SEM (Hitachi S-3500N, Hitachi Science Systems, Ltd., Japan) and TEM (H-7100, Hitachi Co.) were used to study morphology of the samples. For SEM, a piece of each sample was mounted on an aluminum stub, and the surface was coated with a mixture of 60% gold particles and 40% palladium with a sputter coater (Desk II Sputter/Etch Unit, NJ) before observation. For TEM, fine powders of each sample were absorbed onto Formvar/carbon-coated 200-mesh copper grids (Electron Microscopy Sciences, Fort Washington, PA, U.S.A.) and observed without staining.

Differential Scanning Calorimetry (DSC) Analysis. Thermal transitions of the samples were measured with a TA DSC Q200 instrument. About 5 mg of dried powder was sealed in an aluminum pan. An empty sealed pan was used as a reference. The sample was heated from 0 to 190 °C at a rate of 10 °C/min, isothermally conditioned at 190 °C for 3 min, quenched to 0 °C, isothermally conditioned at 0 °C for 3 min, and then heated again to 190 °C at the same rate. The sample was characterized in an inert environment by using nitrogen with a gas flow rate of 50 mL/min. Results were obtained from the second DSC heating scan. Heat capacity (ΔC_p), glass transition temperature (T_g), melting temperature (T_m), heat of melting (ΔH_m), and heat of crystallization (ΔH_c) were determined from the DSC thermograms. Crystallinity (X_m) was estimated according to the equation

$$X_m(\%) = \frac{\Delta H_m}{\Delta H_0} \times 100 \quad (1)$$

Table 1. Molecular Weight and Appearance of PLA, Nanocomposites, and Free PLA

sample	M_w	M_n	PDI[a]	appearance
PLA	42500	23300	1.8	light black fibrils
PLA-0.005%MgO	41900	20000	2.0	slight black fibrils
PLA-0.01%MgO	55500	33000	1.7	white fibrils
PLA-0.05%MgO	26000	14000	1.9	white solids
PLA-0.2%MgO	9400	6300	1.5	white solids
free PLA	10100	6000	1.7	white solids

[a] PDI: Polydispersity index (M_w/M_n).

where ΔH_m and ΔH_0 are heats (J/g) of melting of PLA nanocomposites and PLA crystals of infinite size with a value of 93.6 J/g,[44] respectively.

Thermogravimetric Analysis (TGA). Decomposition characteristics of the samples were determined with a Perkin-Elmer Pyris1 TGA (Norwalk, CT). About 5 mg of each sample was placed in the pan and heated from 40 to 700 °C at a heating rate of 20 °C/min under a nitrogen atmosphere. Pure MgO was dried in a vacuum oven at 80 °C for 24 h before TGA measurement.

Results and Discussion

Molecular Weight. Molecular weights of PLA and bulk nanocomposites are summarized in Table 1. The M_w and M_n of pure PLA were 42500 and 23300, respectively. The M_w and M_n of PLA-0.005%MgO were similar to those of pure PLA, whereas the M_w and M_n of PLA-0.01%MgO were significantly higher than those of pure PLA. When the loading ratio of MgO further increased to 0.05 and 0.2%, M_w decreased sharply by 39 and 78%, respectively, compared with pure PLA. First, the intrinsic balance of carboxyl and hydroxyl groups in lactic acid (−COOH/−OH = 1) was broken by the presence of extra hydroxyl groups on the surface of MgO nanocrystals (−COOH/−OH < 1); therefore, the theoretical molecular weight was reduced at a complete conversion of −COOH. Second, it is known that PLA chains grow from two end groups during polycondensation; however, in the case of nanocomposites, one end group was covalently bonded to the MgO surface, and the chain could grow only from the other end. Third, when several polymer chains grew on the surface of the same MgO nanocrystal, the steric hindrance from neighbor polymer chains increased as the polymer grew.[45] Moreover, the molecular mobility decreased compared with a single free polymer chain, leading to a decrease in chain growth. The increased molecular weight of the PLA-0.01%MgO nanocomposite could be because the decreased size of grafted polymer chains was counterbalanced by the total number of chains on each MgO nanocrystal surface showing a larger hydrodynamic volume at the optimal MgO loading ratio of 0.01%. The PDI for PLA and nanocomposites ranged between 1.5 and 2.0, as measured from GPC; these values are similar to those for PLA obtained from the melt polycondensation method.[24,25]

The molecular weight of free PLA isolated from PLA-*g*-MgO in the PLA-3%MgO nanocomposite was also measured (M_w = 10100 and M_n = 6000). The isolated PLA-*g*-MgO was not very soluble in any solution because of its complicated composition (i.e., aggregates resulted from highly concentrated unreacted MgO nanocrystals, partially reacted MgO nanocrystals, and MgO nanocrystals with different sizes and distribution of grafted PLA chains). Therefore, we failed to measure its molecular weight through GPC. Efforts were made to measure the polymer chain length of PLA-*g*-MgO through solid-state ^{1}H NMR. However, because of the relatively low resolution of solid-state ^{1}H NMR and broad peaks from methyl and methine proton resonances, signals from resonances of methyl or methine

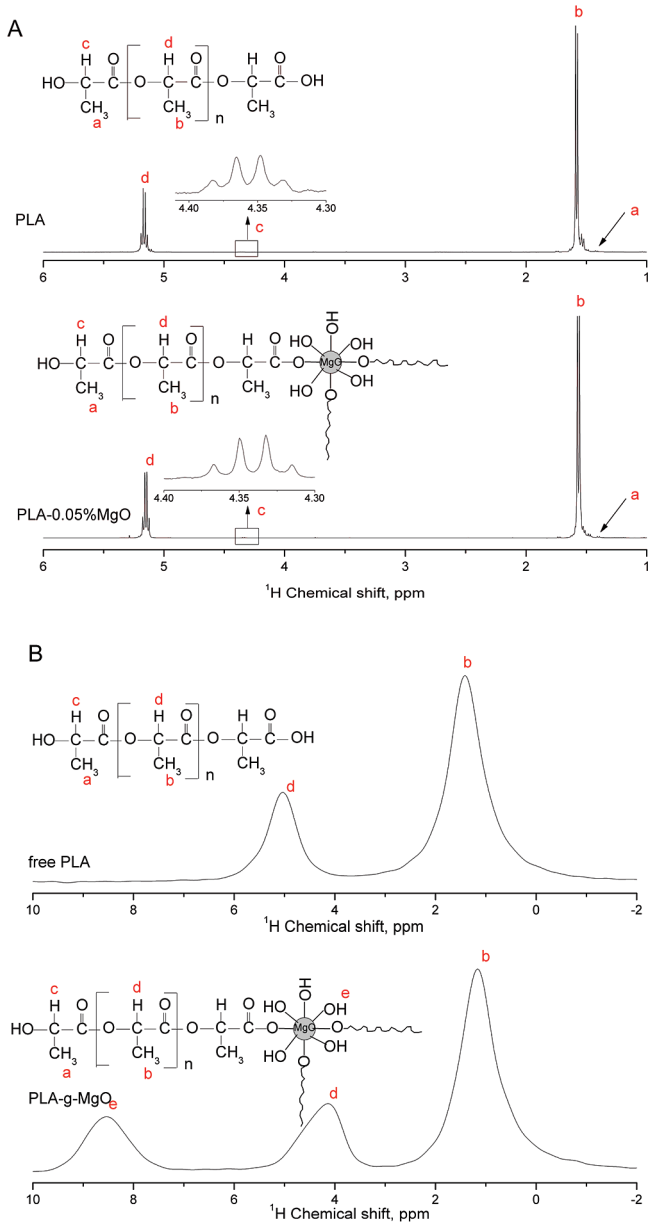

Figure 3. (A) Typical ^{1}H NMR spectra of PLA and nanocomposites; (B) Solid-state ^{1}H NMR spectra of free PLA and PLA-*g*-MgO.

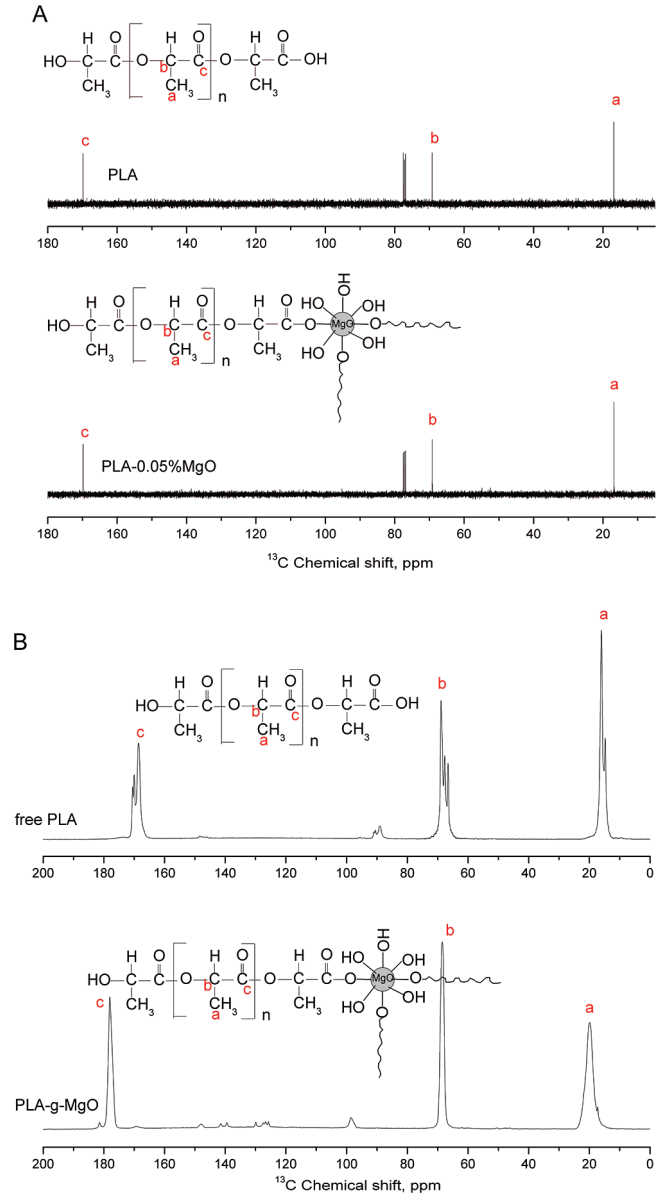

Figure 4. (A) Typical ^{13}C NMR spectra of PLA and nanocomposites; (B) Solid-state ^{13}C NMR spectra of free PLA and PLA-*g*-MgO.

protons next to the terminal hydroxyl groups were not detected. Thus, the chain length of PLA-*g*-MgO was not calculated.

Discoloration of PLA is usually a serious problem in melt polycondensation of lactic acid and might be caused by high reaction temperatures, long reaction times, and byproduct.[24] However, the presence of MgO nanocrystals appears to depress discoloration. Melt polycondensation of lactic acid alone for 10 h resulted in a light black color. With the addition of 0.005% MgO, the color became only slightly black, and with MgO addition further increased to 0.01, 0.05, and 0.2%, the color of nanocomposites became totally white (Table 1). This is probably caused by the specific interaction (chemical grafting, H-bonding, etc.) between PLA and MgO and improved thermal stability of nanocomposites.

NMR. Figure 3A shows the typical ^{1}H NMR spectra of PLA and its bulk nanocomposites. The major peaks at 1.56 and 5.15 ppm were assigned to the methyl and methine proton resonances from the PLA main chain. The weak peak at 4.35 ppm was assigned to the methine proton next to the terminal hydroxyl group. Another weak peak at 1.35 ppm was assigned to the methyl proton next to the terminal hydroxyl group. Peaks assigned to the methyl and methine protons next to the terminal carboxyl group could be identified only for LA oligomers (DP < 8)[46] because the intensity of these peaks decreased dramatically as molecular weight increased and could not be detected. The ^{13}C NMR spectrum was used in a qualitative analysis of the structure of PLA polymers. The result was in accordance with the ^{1}H NMR analysis (Figure 4A). The peaks assigned to the methyl (16.85 ppm), methine (69.21 ppm), and carbonyl (169.81 ppm) groups of the LA repeat units were observed. The three-peak pattern centered at 77 ppm is due to the solvent $CDCl_3$. Resonances associated with methyl, methine, and carbonyl groups next to the terminal hydroxyl or carboxyl groups were not observed because of the relatively long chain length (DP ~165 units, determined from ^{1}H NMR).[47] All the PLA nanocomposites showed ^{1}H and ^{13}C NMR spectra similar to those of pure PLA; the typical spectra of PLA-0.05%MgO is presented in Figures 3A and 4A. Shifts of any peaks attributed to the PLA chains polymerized on the MgO surface were not

detected for these PLA nanocomposites. The same phenomena occurred in multiwalled carbon nanotubes-PLA telechelic prepolymers.[47]

The solid-state ^{1}H NMR spectra for free PLA and PLA-*g*-MgO are shown in Figure 3B. Two broad resonance peaks at 1.41 and 5.03 ppm were attributed to the methyl and methine proton resonances from the main chain of free PLA. In the spectrum of PLA-*g*-MgO, the methyl and methine proton characteristic peaks shifted upfield to 1.16 and 4.13 ppm, respectively, indicating that the chemical environments of methyl and methine protons in the LA repeat units had been changed after being grafted onto the electron-rich MgO surface. A new peak at 8.53 ppm observed only for PLA-*g*-MgO was assigned to the proton resonances from multicoordinated hydroxyl groups of MgO,[37] which possess much lower reactivity. Such differences were also observed in solid-state ^{13}C NMR spectra for free PLA and PLA-*g*-MgO (Figure 4B). The resonances of each of the carbon groups in free PLA were split into two or three distinct peaks, whereas, in PLA-*g*-MgO, almost no split peaks were observed, indicating that a certain degree of racemization occurred for free PLA but little occurred for PLA-*g*-MgO.[24,48,49] The peaks at 169.4, 170.8, and 171.3 ppm that stemmed from carbonyl groups for free PLA shifted to 178 ppm for PLA-*g*-MgO. Another weak peak at 181.4 ppm was probably associated with the terminal carbonyl groups next to the MgO surface. The downfield shift of carbonyl groups might be caused by covalent grafting of PLA chains onto the MgO surface or H-bonding between carbonyl groups and −OH groups from MgO.[50] The peaks at 15.7 and 16.9 ppm assigned to methyl groups for free PLA shifted downfield to 19.9 ppm for PLA-*g*-MgO. NMR results revealed a great possibility that PLA chains were chemically grafted onto the MgO surface, which was also confirmed by other techniques as described in the following paragraphs.

FTIR. The FTIR spectra of pure PLA and bulk nanocomposites are presented in Figure 5A. Pure PLA showed a strong absorption band at 1751 cm^{-1} (Figure 5A, a) corresponding to the stretching vibration of carbonyl groups (-C═O) from the repeated ester units. The -C−O- stretching vibrations from the ester units were observed at 1180, 1129, and 1082 cm^{-1}. The bands at 2996 and 2877 cm^{-1} were assigned to the -C−H asymmetric and symmetric stretching vibrations of CH_3 groups in the side chains, whereas their bending vibration was observed at 1454 cm^{-1}. The band at 2948 cm^{-1} was attributed to the stretching of −CH- groups in the main chain of PLA, and its symmetric and asymmetric bending vibrations appear at 1382 and 1358 cm^{-1}.[51]

Similar FTIR bands were observed for PLA bulk nanocomposites, except for the -C═O region around 1751 cm^{-1} (Figure 5A). In the nanocomposites (b−e), the stretching vibrations of -C═O were all split into two distinct peaks, unlike the single carbonyl peak of pure PLA (Figure 5A, a). One of the split peaks at about 1751 cm^{-1} was still assigned to the original -C═O vibration, which is free and not H-bonding with MgO nanocrystals; the other peak shifted to a lower wavenumber around 1745 to 1747 cm^{-1} and was caused by the formation of intermolecular H-bonding, as illustrated in Figure 1. The H-bonding involves -C═O groups from both grafted and free PLA chains, which are often regarded as H-bonding acceptors, together with some remaining −OH groups from the MgO nanocrystal surface, which are usually considered H-bonding donors. The abundance of surface −OH groups of MgO nanocrystals provided a favorable condition for formation of H-bonding. The H-bonding between PLA and other −OH rich materials observed through FTIR was also reported in other studies.[52,53]

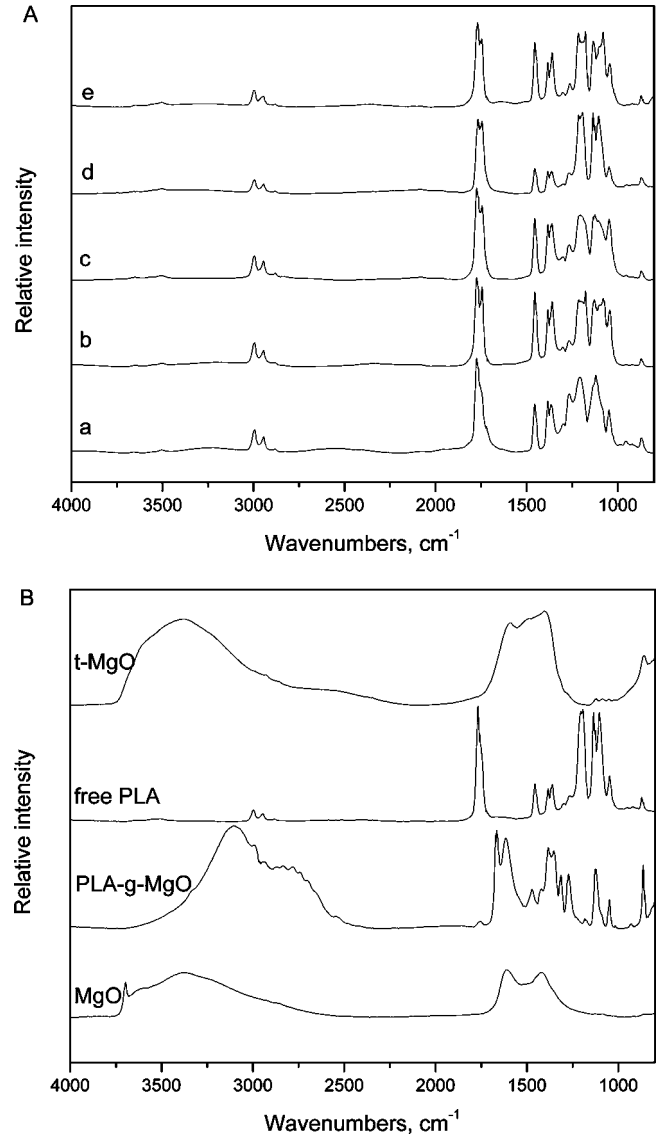

Figure 5. FTIR spectra of (A) PLA and nanocomposites (a, PLA; b, PLA-0.005%MgO; c, PLA-0.01%MgO; d, PLA-0.05%MgO; e, PLA-0.2%MgO); (B) MgO, PLA-*g*-MgO, free PLA, and t-MgO (a comparative sample, see text).

Compared with MgO, PLA-*g*-MgO showed new absorption bands at 1751, 2990, and 2940 cm^{-1} (Figure 5B). These peaks were attributed to the -C═O, $-CH_3$, and −CH− groups, respectively, from PLA chains grafted onto the MgO nanocrystals. The spectrum of t-MgO was in accordance with that of pure MgO, and no characteristic peaks of PLA were observed. The −OH absorption band of PLA-*g*-MgO was different from that of MgO and t-MgO. In particular, the 3500−3800 cm^{-1} signal disappeared after surface grafting. This was caused by selective grafting of PLA with the mono- and dicoordinated −OH groups[54] because of their higher reactivity, which was discussed previously. These results confirm that PLA chains were chemically grafted onto the MgO surface.

Morphology. The SEM images of MgO, pure PLA, bulk nanocomposites, and PLA-*g*-MgO are shown in Figure 6. The bare MgO crystals existed in compact aggregate forms with an average size of 10−15 μm. PLA exhibited incontinuous particular morphology with a flat, smooth surface (Figure 6a).

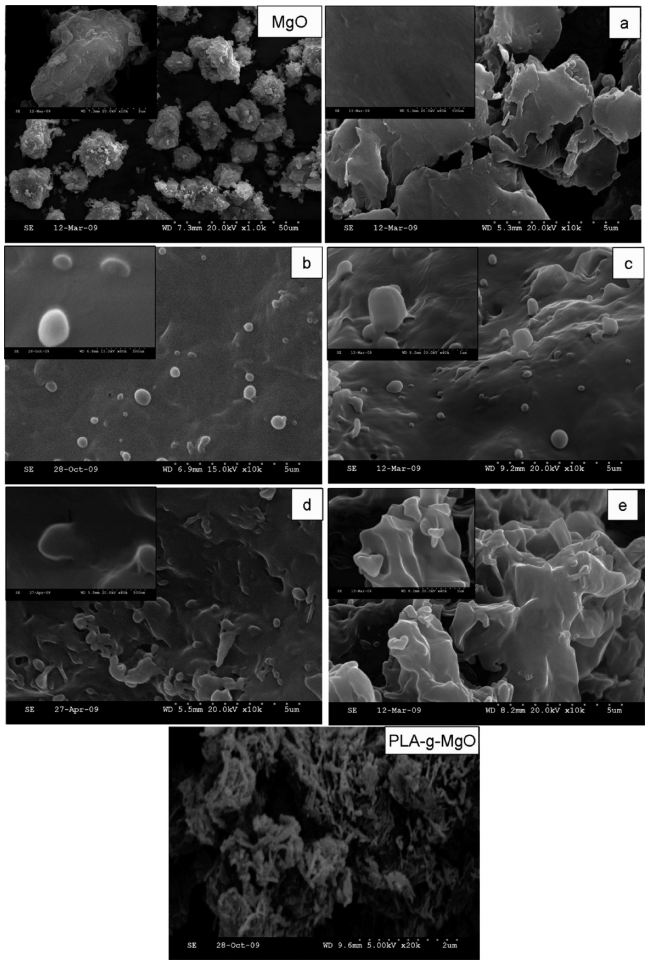

Figure 6. SEM images of MgO, PLA, nanocomposites (a, PLA; b, PLA-0.005%MgO; c, PLA-0.01%MgO; d, PLA-0.05%MgO; e, PLA-0.2%MgO), and PLA-*g*-MgO (scale bar is shown at the bottom of each image).

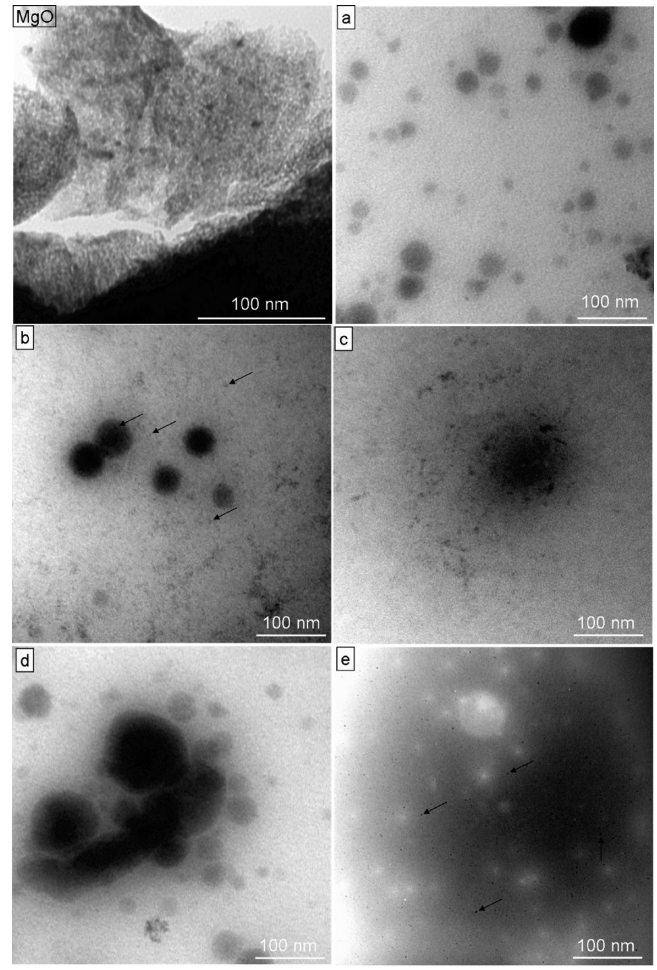

Figure 7. TEM images of MgO, PLA, and nanocomposites (a, PLA; b, PLA-0.005%MgO; c, PLA-0.01%MgO; d, PLA-0.05%MgO; e, PLA-0.2%MgO).

All the bulk nanocomposites exhibited continuous morphology with small, uniformly distributed convexities (Figure 6b−e). As MgO loading ratio increased, the number of convexities per unit area in the nanocomposite matrix obviously increased. At 0.2% MgO, the convexities grew and aggregated together, resulting in a more irregular and uneven surface. The convexities resulting from PLA-*g*-MgO nanocomposites were uniformly dispersed in the matrix with a remarkably reduced size (100−500 nm), which indicates that initial MgO aggregates were effectively broken down to nanoscale through in situ polymerization. In addition to nanoscale uniform dispersion, interfacial interaction is another key factor for nanocomposite preparation. As seen from Figure 6b−e, the smooth, continuous feature at the interface between the PLA matrix and convexities indicates that a chemical reaction occurred between PLA and MgO. In general, chemical grafting of polymer chains that are compatible with the polymer matrix on the inorganic particles provides strong interfacial interaction between the inorganic and the organic phases.[55] Moreover, the formation of H-bonding between organic PLA chains and inorganic nanocrystals contributes to the unique continuousness observed only in the bulk nanocomposites and further improves the interfacial interaction. PLA-*g*-MgO exhibited a unique loose and porous morphology (Figure 6), indicating that the compact aggregation of original MgO crystals was greatly inhibited after surface grafting with PLA chains.

TEM is more a powerful technique than SEM for penetrating the surrounding polymer environment and provides information about how MgO nanocrystals were distributed inside each convexity observed in the SEM images. Before polymerization, bare MgO crystals severely aggregated, and it was difficult to distinguish a single crystal (Figure 7, MgO). After it was grafted with PLA, the surface-grafted MgO was almost homogeneously dispersed in the polymer matrix without obvious aggregation and kept its nanostructures with individual MgO crystals (pointed arrows in Figure 7b). These results indicate that agglomeration of nanocrystals was prevented by the surface grafting and H-bonding between PLA chains and surface hydroxyl groups of MgO, which also afforded the uniform dispersion. When MgO incorporation increased to 0.01 and 0.05%, the abundant OH groups were prone to interact with themselves because of the stronger intramolecular hydroxyl−hydroxyl bonding;[52] this led to a small amount of aggregation of several MgO crystals, but the aggregation was slight and incompact (Figure 7c,d). When the MgO loading ratio further increased to 0.2%, much denser and thicker black spots were observed (pointed arrow in Figure 7e), indicating that large, compact aggregates of MgO crystals were formed. PLA-*g*-MgO exhibited a unique fibril structure due to the surface-grafted polymer chains (Figure 8, left), which was obviously different from the morphology of pure MgO (Figure 7, MgO). At higher magnification, uniform distribution of MgO crystals in the PLA-*g*-MgO system was also observed (Figure 8, right).

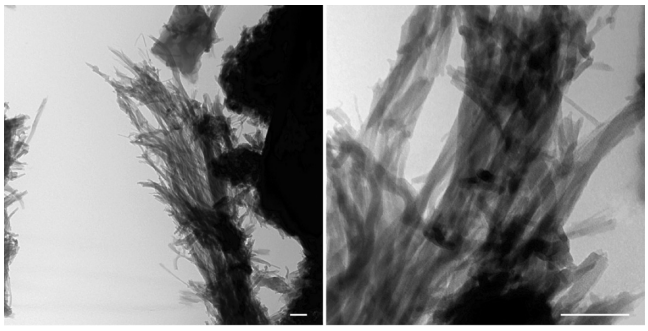

Figure 8. TEM images of PLA-*g*-MgO (left: lower magnification, 34000×; right: higher magnification, 130000×; scale bar: 100 nm).

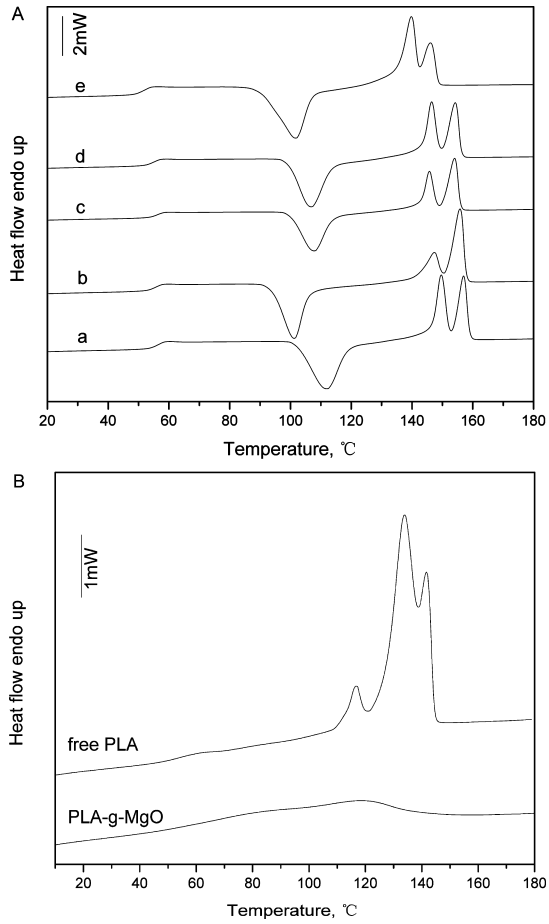

Figure 9. DSC thermograms of (A) PLA and nanocomposites (a, PLA; b, PLA-0.005%MgO; c, PLA-0.01%MgO; d, PLA-0.05%MgO; e, PLA-0.2%MgO); and (B) free PLA and PLA-*g*-MgO.

Thermal Properties. Figure 9A shows the DSC thermograms of pure PLA and bulk nanocomposites, and quantified results are summarized in Table 2. Pure PLA and bulk nanocomposites showed similar T_g values, except for PLA-0.2%MgO. The T_g of PLA-0.2%MgO was about 4 °C lower than that of other nanocomposites because of its smaller molecular weight.[56]

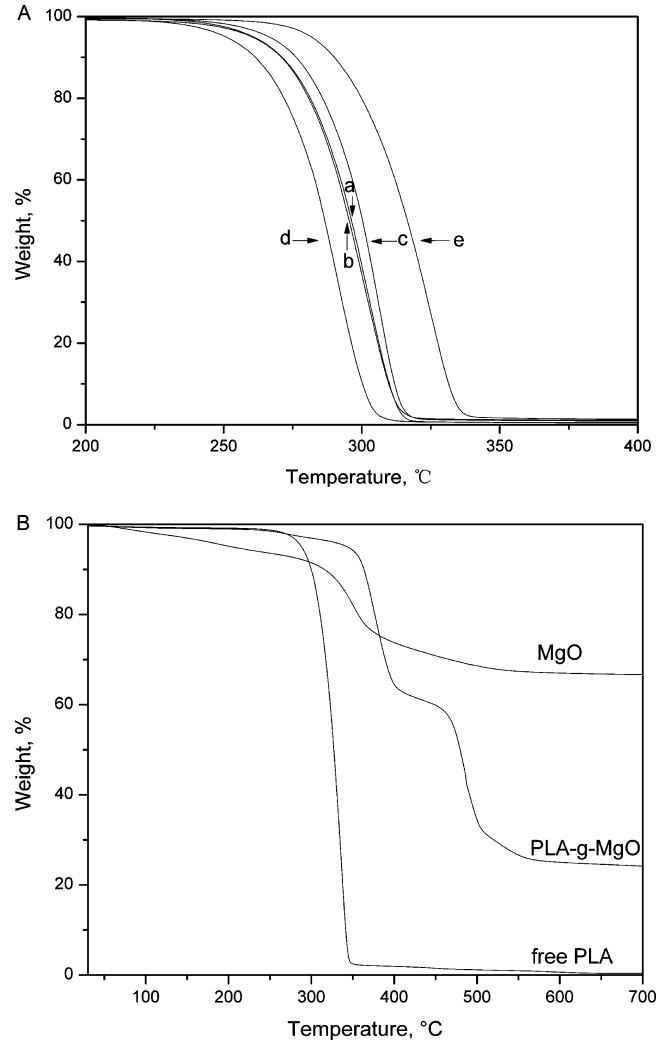

Figure 10. TGA of (A) PLA and nanocomposites (a, PLA; b, PLA-0.005%MgO; c, PLA-0.01%MgO; d, PLA-0.05%MgO; e, PLA-0.2%MgO); and (B) MgO, PLA-*g*-MgO, and free PLA.

Cold crystallization was observed for PLA and the bulk nanocomposites. Compared with PLA, the cold crystallization of bulk nanocomposites occurred at lower temperatures. The depression of cold crystallization temperature in the bulk nanocomposites was probably induced by the MgO nanocrystals, which acted as nucleation agents for the system. No obvious change of crystallinity was observed between PLA and bulk nanocomposites, except for PLA-0.01%MgO, which showed relatively lower crystallinity. As discussed previously, the PLA-0.01%MgO nanocomposite had the highest molecular weight because optimal size and number of grafted PLA chains were obtained. However, a 0.01% MgO nanocrystal core might hinder mobility of the grafted PLA chain and limit the effective diffusion of chains to the growing crystalline lamella, resulting in crystals with reduced grain size, more defects, and, therefore,

Table 2. Thermal Properties of PLA, Nanocomposites, Free PLA, and PLA-*g*-MgO Determined from DSC Thermograms

sample	T_g (°C)	ΔC_p [J/(g·°C)]	T_c (°C)	ΔH_c (J/g)	T_m (°C)	ΔH_m (J/g)	X_m (%)
PLA	55.9	0.63	112.0	−42.6	149.6, 157.0	44.2	47.2
PLA-0.005%MgO	55.3	0.62	101.2	−42.1	147.3, 155.8	44.2	47.3
PLA-0.01%MgO	55.9	0.59	107.8	−37.9	145.7, 154.0	38.5	41.1
PLA-0.05%MgO	54.6	0.59	106.8	−42.0	146.5, 154.3	42.2	45.0
PLA-0.2%MgO	51.4	0.62	101.7	−41.5	139.8, 146.2	43.3	46.3
free PLA	54.8	0.17			116.4, 133.7, 141.6	52.8	56.4
PLA-*g*-MgO					117.8		

Table 3. Thermal Decomposition Temperatures of PLA, Nanocomposites, Free PLA, MgO, and PLA-*g*-MgO Derived from TGA Thermograms

sample	T_{onset} (°C)	T_{end} (°C)	T_{max} (°C)
PLA	278.5	317.1	302.4
PLA-0.005%MgO	278.8	316.5	301.4
PLA-0.01%MgO	287.3	317.2	306.5
PLA-0.05%MgO	268.5	307.2	292.1
PLA-0.2%MgO	296.2	338.0	324.0
free PLA	305.7	346.8	336.0
MgO	50.9, 160.7, 310.9	117.1, 213.9, 379.5	73.4, 184.4, 350.8
PLA-*g*-MgO	267.6, 353.3, 463.4	297.7, 404.9, 508.7	270.9, 376.2, 484.7

lower crystallinity. Both PLA and bulk nanocomposites exhibited double melting behavior, which can be explained by the melt-recrystallization model.[57] The melting temperatures of bulk nanocomposites were all lower than that of pure PLA, especially that of PLA-0.2%MgO, which was 10 °C lower. The sharp reduction of melting temperature for PLA-0.2%MgO was caused by its lower molecular weight.[58]

DSC thermograms of free PLA and PLA-*g*-MgO isolated from the PLA-3%MgO nanocomposite are presented in Figure 9B, and the results are also summarized in Table 2. PLA-*g*-MgO showed a broad melting peak with a peak value of 117.8 °C. For free PLA, besides the normal double melting peaks at 133.7 and 141.6 °C, another small melting peak was observed at 116.4 °C, indicating there were still some PLA-*g*-MgO residues dissolved/dispersed in the chloroform solution with free PLA during the isolation process.

The TGA thermograms of pure PLA and bulk nanocomposites are presented in Figure 10A, and the thermogravimetric data are summarized in Table 3. The onset, end, and maximum rate of decomposition temperatures (T_{onset}, T_{end}, and T_{max}) of PLA and PLA-0.005%MgO were similar. PLA-0.01%MgO exhibited increased thermal stability compared with pure PLA. The thermal stability of PLA-0.05%MgO was the lowest, with T_{onset}, T_{end}, and T_{max} about 10 °C lower than those for pure PLA. The T_{max} for PLA-0.2%MgO was 324 °C, which was the highest among all samples. These results indicate that addition of MgO could increase thermal stability of PLA. The decreased thermal stability of PLA-0.05%MgO could be explained by the competition between the addition of MgO and the decrease in molecular weight.

The TGA thermograms of intensively dried pure MgO, PLA-*g*-MgO, and free PLA are presented in Figure 10B, and thermogravimetric data are summarized in Table 3. The weight loss of MgO (W_{MgO}) and PLA-*g*-MgO ($W_{PLA\text{-}g\text{-}MgO}$) was 33.3 and 75.8%, respectively. The amount of PLA grafted onto the MgO surface (W_g) for PLA-*g*-MgO was roughly calculated as:

$$W_g = W_{PLA\text{-}g\text{-}MgO} - W_{MgO} = 75.8\% - 33.3\% = 42.5\% \quad (2)$$

The amount of −OH groups on the MgO surface involved in the surface grafting was neglected in this calculation, which indicates that more than 42.5% PLA was successfully grafted. The decomposition range of MgO and PLA-*g*-MgO both exhibited three stages, with T_{max} at 73, 184, and 351 °C for MgO and 271, 376, and 485 °C for PLA-*g*-MgO. The detailed mechanism for the decomposition of PLA-*g*-MgO remains unclear. However, we can conclude that when PLA was grafted onto MgO, its thermal stability was greatly improved. Moreover, because free PLA has some PLA-*g*-MgO not separated thoroughly, the T_{max} was 34 °C higher than that of pure PLA, even though the molecular weight of free PLA was much lower than that of pure PLA.

Conclusions

PLA-MgO nanocomposites were synthesized by in situ melt polycondensation of LA and surface-hydroxylated MgO nanocrystals at a low MgO loading level. Molecular weight of the PLA-0.01%MgO reached 55500, which was 30% higher than that of pure PLA. The color of PLA-MgO nanocomposites was almost white, whereas that of pure PLA was slightly black.

PLA-MgO nanocomposites exhibited continuous morphology with small convexities uniformly distributed in the matrix because of surface grafting and H-bonding between PLA chains and hydroxylated MgO. Pure PLA exhibited an incontinuous particle morphology with a flat, smooth surface. MgO crystals acted as nucleation agents to induce and accelerate crystallization of the PLA-MgO nanocomposite. Decomposition of the PLA-MgO nanocomposite was significantly increased compared with that of pure PLA. Results indicate this is a promising approach to preparing PLA/MgO nanocomposites.

Acknowledgment. Financial support was provided from U.S. Department of Agriculture/National Research Initiative and U.S. Department of Energy. Contribution No. 10-278-J from the Kansas Agricultural Experiment Station. The authors gratefully acknowledge the following individuals for their contributions: Dr. Krystyna Brzezinska and Dr. Jerry Hu (Materials Research Laboratory at UCSB) for performing GPC and solid-state NMR analysis, Dr. David Wetzel (Department of Grain Science and Industry, Kansas State University) for use of the FTIR instrument, Mr. Kent Hampton (Department of Entomology, Kansas State University) for performing SEM analysis, and Dr. Dan Boyle (Department of Biology, Kansas State University) for performing TEM analysis.

References and Notes

(1) Anderson, K. S.; Schreck, K. M.; Hillmyer, M. A. *Polym. Rev.* **2008**, *48*, 85–108.
(2) Gupta, A. P.; Kumar, V. *Eur. Polym. J.* **2007**, *43*, 4053–4074.
(3) Ljungberg, N.; Wesslen, B. *Biomacromolecules* **2005**, *6*, 1789–1796.
(4) Zhang, J.; Sun, X. S. *Biomacromolecules* **2004**, *5*, 1446–1451.
(5) Gacitua, W.; Ballerini, A. A.; Zhang, J. *Maderas: Cienc. Tecnol.* **2005**, *7*, 159–178.
(6) Vaia, R. A.; Jandt, K. D.; Kramer, E. J.; Giannelis, E. P. *Chem. Mater.* **1996**, *8*, 2628–2635.
(7) Alexandre, M.; Dubois, P. *Mater. Sci. Eng., R* **2000**, *28*, 1–63.
(8) Yang, K.; Wang, X.; Wang, Y. *J. Ind. Eng. Chem.* **2007**, *13*, 485–500.
(9) Ray, S. S.; Bousmina, M. *Prog. Mater. Sci.* **2005**, *50*, 962–1079.
(10) Ray, S. S.; Okamoto, M. *Prog. Polym. Sci.* **2003**, *28*, 1539–1641.
(11) Zou, H.; Wu, S.; Shen, J. *Chem. Rev.* **2008**, *108*, 3893–3957.
(12) Tingaut, P.; Zimmermann, T.; Lopez-Suevos, F. *Biomacromolecules* **2010**, *11*, 454–464.
(13) Haque, S.; Rehman, I.; Darr, J. A. *Langmuir* **2007**, *23*, 6671–6676.
(14) Luo, Y.; Wang, X.; Xu, D.; Wang, Y. *Appl. Surf. Sci.* **2009**, *255*, 6795–6801.
(15) Ray, S. S.; Maiti, P.; Okamoto, M.; Yamada, K.; Ueda, K. *Macromolecules* **2002**, *35*, 3104–3110.
(16) Chen, G.; Kim, H.; Shim, J.; Yoon, J. *Macromolecules* **2005**, *38*, 3738–3744.
(17) Wang, B.; Sun, X. S.; Klabunde, K. J. *J. Biobased Mater. Bioenergy* **2009**, *3*, 130–138.
(18) Hong, Z.; Qiu, X.; Sun, J.; Deng, M.; Chen, X.; Jing, X. *Polymer* **2004**, *45*, 6699–6706.
(19) Feng, J.; Cai, W.; Sui, J.; Li, Z.; Wan, J.; Chakoli, A. N. *Polymer* **2008**, *49*, 4949–4994.

(20) Paul, M. A.; Delcourt, C.; Alexandre, M.; Degée, P.; Monteverde, F.; Rulmont, A.; Dubois, P. *Macromol. Chem. Phys.* **2005**, *206*, 484–498.
(21) Rong, M. Z.; Zhang, M. Q.; Ruan, W. H. *Mater. Sci. Technol.* **2006**, *22*, 787–796.
(22) Mehta, R.; Kumar, V.; Bhunia, H.; Upadhyay, S. *J. Macromol. Sci., Part C: Polym. Rev.* **2005**, *45*, 325–349.
(23) Garlotta, D. *J. Polym. Environ.* **2001**, *9*, 63–84.
(24) Moon, S. I.; Lee, C. W.; Miyamoto, M.; Kimura, Y. *J. Polym. Sci., Polym. Chem.* **2000**, *38*, 1673–1679.
(25) Moon, S. I.; Kimura, Y. *Polym. Int.* **2003**, *52*, 299–303.
(26) Moon, S. I.; Lee, C. W.; Taniquchi, I.; Miyamoto, M.; Kimura, Y. *Polymer* **2001**, *42*, 5059–5062.
(27) Al-Abadleh, H. A.; Grassian, V. H. *Surf. Sci. Rep.* **2003**, *52*, 63–161.
(28) Henderson, M. A. *Surf. Sci. Rep.* **2002**, *46*, 1–308.
(29) Richards, R.; Li, W.; Decker, S.; Davidson, C.; Koper, O.; Zaikovski, V.; Volodin, A.; Rieker, T.; Klabunde, K. J. *J. Am. Chem. Soc.* **2000**, *122*, 4921–4925.
(30) Yan, S.; Yin, J.; Yang, Y.; Dai, Z.; Ma, J.; Chen, X. *Polymer* **2007**, *48*, 1688–1694.
(31) Wu, L.; Cao, D.; Huang, Y.; Li, B. *Polymer* **2008**, *49*, 742–748.
(32) Yao, X.; Tian, X.; Xie, D.; Zhang, X.; Zheng, K.; Xu, J.; Zhang, G.; Cui, P. *Polymer* **2009**, *50*, 1251–1256.
(33) Lu, X.; Lv, X.; Sun, Z.; Zheng, Y. *Eur. Polym. J.* **2008**, *44*, 2476–2481.
(34) Langel, W.; Parrinello, M. *Phys. Rev. Lett.* **1994**, *73*, 504–507.
(35) Kim, Y. D.; Stultz, J.; Goodman, D. W. *J. Phys. Chem. B* **2002**, *106*, 1515–1517.
(36) Chizallet, C.; Costentin, G.; Lauron-Pernot, H.; Krafft, J. M.; Bazin, P.; Saussey, J.; Delbecq, F.; Sautet, P.; Che, M. *Oil Gas Sci. Technol.* **2006**, *61*, 479–488.
(37) Chizallet, C.; Costentin, G.; Lauron-Pernot, H.; Che, M.; Bonhomme, C.; Maquet, J.; Delbecq, F.; Sautet, P. *J. Phys. Chem. C* **2007**, *111*, 18279–18287.
(38) Huang, C. C.; Hohn, K. L.; Schlup, J. R. *J. Phys. Chem C* **2009**, *113*, 11050–11059.
(39) Utamapanya, S.; Klabunde, K. J.; Schlup, J. R. *Chem. Mater.* **1991**, *3*, 175–181.
(40) Itoh, H.; Utamapanya, S.; Stark, J. V.; Klabunde, K. J.; Schlup, J. R. *Chem. Mater.* **1993**, *5*, 71–77.
(41) Lucas, E.; Decker, S.; Khaleel, A.; Seitz, A.; Fultz, S.; Ponce, A.; Li, W.; Carnes, C.; Klabunde, K. J. *Chem.—Eur. J.* **2001**, *7*, 2505–2510.
(42) Neal, L. M.; Hernandez, D.; Hagelin-Weaver, H. E. *J. Mol. Catal. A: Chem.* **2009**, *307*, 29–36.
(43) Beavers, E. M.; Klabunde, K. J.; Wang, B.; Sun, X. S. *New J. Chem.* **2009**, *33*, 1951–1959.
(44) Fischer, E. W.; Sterzel, H. J.; Wegner, G. *Kolloid Z. Z. Polym.* **1973**, *251*, 980–990.
(45) Zhao, H.; Kang, X.; Liu, L. *Macromolecules* **2005**, *38*, 10619–10622.
(46) Espartero, J. L.; Rashkov, I.; Li, S. M.; Manolova, N.; Vert, M. *Macromolecules* **1996**, *29*, 3535–3539.
(47) Song, W.; Zheng, Z.; Lu, H.; Wang, X. *Macromol. Chem. Phys.* **2008**, *209*, 315–321.
(48) Thakur, K. A. M.; Kean, R. T.; Hall, E. S.; Kolstad, J. J.; Lindgren, T. A.; Doscotch, M. A.; Siepmann, J. I.; Munson, E. J. *Macromolecules* **1997**, *30*, 2422–2428.
(49) Kricheldorf, H. R.; Boettcher, C.; Tonnes, K. U. *Polymer* **1992**, *33*, 2817–2824.
(50) Ando, S.; Ando, I.; Shoji, A.; Ozaki, T. *J. Am. Chem. Soc.* **1988**, *110*, 3380–3386.
(51) Auras, R.; Harte, B.; Selke, S. *Macromol. Biosci.* **2004**, *4*, 835–864.
(52) Lin, Y.; Zhang, K.; Dong, Z.; Dong, L.; Li, Y. *Macromolecules* **2007**, *40*, 6257–6267.
(53) Zhou, S.; Zheng, X.; Yu, X.; Wang, J.; Weng, J.; Li, X.; Feng, B.; Yin, M. *Chem. Mater.* **2007**, *19*, 247–253.
(54) Chizallet, C.; Costentin, G.; Che, M.; Delbecq, F.; Sautet, P. *J. Am. Chem. Soc.* **2007**, *129*, 6442–6452.
(55) Hong, Z.; Zhang, P.; He, C.; Qiu, X.; Liu, A.; Chen, L.; Chen, X.; Jing, X. *Biomaterials* **2005**, *26*, 6296–6304.
(56) Jamshidi, K.; Hyon, S. H.; Ikada, Y. *Polymer* **1988**, *29*, 2229–2234.
(57) Yasuniwa, M.; Tsubakihara, S.; Sugimoto, Y.; Nakafuku, C. *J. Polym. Sci., Polym. Phys.* **2004**, *42*, 25–32.
(58) Ikada, Y.; Tsuji, H. *Macromol. Rapid Commun.* **2000**, *21*, 117–132.

BM100320Q